PROCEEDINGS, 47th Workshop on Geothermal Reservoir Engineering
Stanford University, Stanford, California, February 7-9, 2022
SGP-TR-223

New Large-Scale Passive Seismic Monitoring at The Geysers Geothermal Reservoir, CA, USA

Roland Gritto[1], Steve P. Jarpe[2], David L. Alumbaugh[3]

[1]Array Information Technology, 2020 Cedar Street, Berkeley, CA 94709

[2]Jarpe Data Solutions Inc., Prescott Valley, AZ 86314

[3]Lawrence Berkeley National Laboratory, Berkeley, CA 94720

Roland.Gritto@arrayinfotech.com

Keywords: geothermal reservoir, dense seismic array, seismic reservoir imaging

ABSTRACT

In this paper, we present preliminary results for reservoir-wide passive seismic monitoring at The Geysers geothermal reservoir combining data from two seismic networks. The combined network with 139 stations comprises the permanently installed BG network with 49 stations and the recently installed temporary CEC network with 90 stations. For the first time, the combined network offers the opportunity to monitor the geological structure and reservoir heterogeneity on a large scale and with high resolution of the seismic velocities. During the current project, seismic imaging will be conducted on an annual basis and potential temporal changes analyzed to study the underlying reservoir processes. The study area comprises the whole reservoir with an approximate extent of 30 km in NW-SE direction and 15 km in SW-NE direction. We present results for a one-year period from more than 30,000 earthquakes that were automatically processed for P- and S-wave phase arrival times. The data were subsequently inverted using a joint inversion approach to image the spatial heterogeneity of the reservoir including the 3D P- and S-wave velocity structure, Vp/Vs-ratio, and earthquake hypocenter locations. While the P- and S-wave velocity estimates reveal the geological structure of the reservoir, the Vp/Vs-ratio can be used to deduce the state of the fluid saturation (water vs. steam) in the reservoir. The seismic data will eventually be combined with reservoir wide magnetotelluric (MT) measurements to conduct joint MT and seismic imaging using workflows and algorithms that enforce structural similarity constraints between the different physical properties. The joint inversion of the multi-physics data can yield reservoir structure with higher spatial certainty than either of the data sets by themselves, which would improve the capability to quantify the response of an operating geothermal field to changes in injection and production.

1. INTRODUCTION

Past studies of geothermal reservoirs have shown that seismic velocity measurements and specifically the ratio between P- and S-wave velocity (Vp/Vs-ratio) can be used to map regions of gas versus liquid saturation. Applications include imaging fluids such as oil, water, and CO_2 in second and tertiary oil recovery (Gritto et al., 2004), tracing the movement of fluids associated with volcanic swarms (Dahm and Fischer, 2013), imaging fluids in fault zones (Lin and Shearer, 2007) and mapping the presence of liquid and gaseous fluids in geothermal reservoirs (Lin and Shearer, 2009; Gritto et al., 2013a; Gritto and Jarpe, 2014). In a passive seismic tomography study at The Geysers geothermal reservoir, Gritto et al. (2013b) showed regions of low Vp/Vs correlating with areas of high steam saturation, while high Vp/Vs-ratios were found in regions that were subjected to high rates of water injection to rehydrate the reservoir. In a recent study, Gritto et al. (2020) utilized a temporary deployment of cost-effective seismic sensors with dense station coverage to image the structural controls, and the presence of water and steam in the northwest Geysers. In the current study, we combine the temporary dense seismic network with the permanently installed seismic network to obtain the highest resolution and the best spatial coverage to date to improve the seismic imaging results at The Geysers geothermal reservoir. Furthermore, the current study has the goal to conduct multi-physics data inversion, using MT (Peacock et al., 2022) and passive seismic imaging, to obtain reservoir structure with improved certainty in the structural controls and in the locations of water and steam in the reservoir. The joint inversion will be performed using workflows and algorithms that enforce structural similarity constraints between the different physical properties (Um et al., 2014).

2. SEISMIC NETWORKS AND DATA PROCESSING

The seismic network comprises 139 stations, combining 90 seismic stations from the recently installed temporary California Energy Commission (CEC) network and 49 stations from the permanently installed Berkeley Geysers (BG) network. The intention of combining seismic data from these networks included the improved spatial coverage and resolution during passive seismic tomographic imaging. A map of the combined seismic network is presented in Figure 1, where the outline of the steam field is given by the red polygon and the surface traces of the known faults are indicated by the black lines. The locations of the 90 temporary CEC-network stations and of the 49 permanent BG-network stations are shown, respectively, by the red and green triangles. While the BG network covers the entire reservoir, the CEC network was deployed in the northwest Geysers to support the development of Calpine's operation in this area.

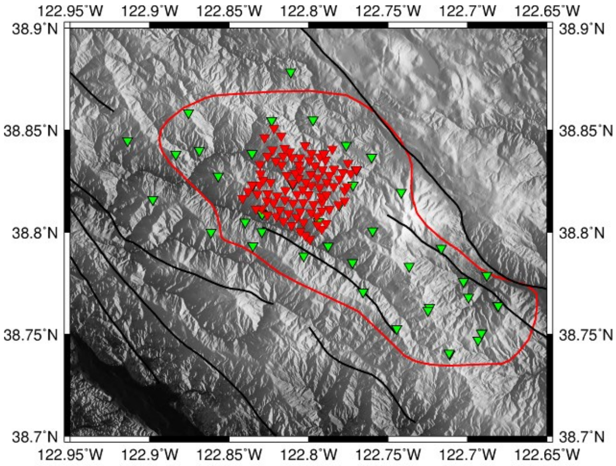

Figure 1: The 139-station seismic network at The Geysers geothermal reservoir consisting of 91 CEC-network stations (red triangles) and 49 BG-network stations (green triangles).

A picture of a temporary deployed CEC seismic station is presented in Figure 2a. Wherever possible, these stations were deployed on rock outcrops throughout a 5 km by 5 km region in the northwest Geysers. The stations comprise three-component 4.5 Hz geophone sensors to record the ground motion, a solar panel and 12 V battery for power supply, and a GPS antenna for timing. While the design of the seismic stations includes a mobile phone circuit board for automatic data transmission, the lack of mobile network coverage at The Geysers requires data storage on SD memory cards and regular data collection on a quarterly basis. The permanently deployed BG network has been in operation for several decades and has been expanded and upgraded multiple times. At present, it comprises 49 surface and shallow borehole stations with 4.5 Hz and 2Hz three-component sensors. In contrast to the temporary stations, data from the BG stations are telemetered by radio antennas to a computer at a local facility, where the seismic data are preprocessed and transmitted to a processing center for further analysis. A picture of a permanent seismic station is presented in Figure 2b. The components of the stations are mounted on a pole, with a radio antenna for data transmission at the top. The solar panel supplies power for the electronics, which are housed in the gray box below. The box contains batteries, a GPS unit for time keeping, and a digitizer. The three-component sensors is buried below the surface at the base of the pole.

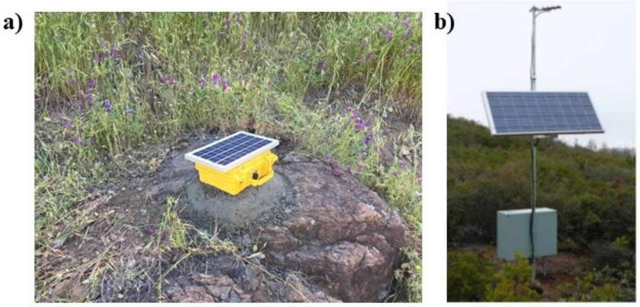

Figure 2: a) Site of a temporarily deployed seismic station. b) Site of a permanently deployed seismic station.

Seismic data processing is performed based on the Rapid Earthquake Monitoring and Analysis System REMAS (Hutchings et al., 2011) and PhaseNet (Zhu and Berosa, 2019) software packages, which perform fast, automated processing of micro-earthquake data from dense networks. This software provides complete data processing including phase detection, event association and location, estimation of phase travel time, pulse width, event moment magnitude, seismic moment, generation of waveforms, and storage of parameters in a database.

In the current paper, we present the results from the analysis of seismic data collected between May 2018 and June 2019. Data processing using REMAS and PhaseNet resulted in the detection and preliminary location of 32,000 events with 1,200,000 P-wave and 1,000,000 S-wave phase arrivals. The moment magnitude of the events ranged between -1.5 and +2.9 as shown in Figure 3. It can be seen that the maximum number of detected events have a moment magnitude of 0.3 Mw. This shows the challenge of analyzing events at The Geysers, where most of the events have magnitude at or below the magnitude of completeness (Mc). The magnitude of completeness defines a limit at which a network detects all events with magnitudes equal or higher than Mc. However, the network still detects some events with magnitudes lower than Mc. As reported by Layland-Bachmann et al. (2019), the magnitude of completeness for the CEC- and BG-network is Mc=0.5 and Mc=1.0, respectively. This indicates that most of the events processed during the current data collection period were detected by the CEC-network, which is not surprising, since the CEC network with high-density station coverage is designed to detect events with small magnitudes over an area with relatively small footprint (i.e., 5x5 km area). The number of events decay quickly for magnitudes smaller than Mc due to high ambient noise levels at the geothermal reservoir, including active steam and water pipelines, power stations, traffic, and maintenance work. The upper limit Mw 2.5 is governed by the tectonic regime, which limits the occurrence of larger magnitudes to longer time periods.

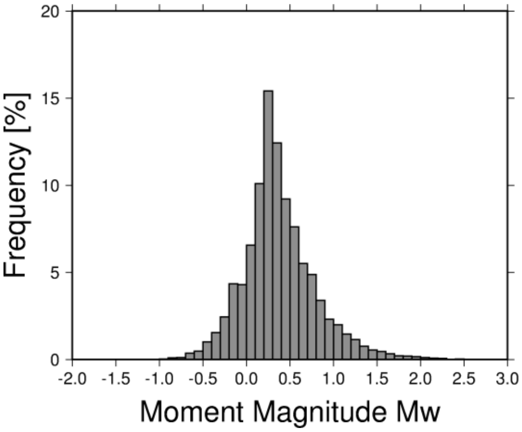

Figure 3: Histogram of moment magnitude Mw of 32,000 events recorded between May 2018 and June 2019.

3. THREE-DIMENSIONAL SEISMIC IMAGING FOR P- AND S-WAVE VELOCITY STRUCTURE AND V_P/V_S-RATIO

The seismic phase data and preliminary earthquake locations were used in a joint inversion to derive earthquake hypocenter locations and 3D distributions of the P- and S-wave velocity structure in the reservoir. The inversion code, tomoFDD, takes advantage of dynamic memory allocation, which is important for seismic imaging at The Geysers, where high volumes of seismic travel time data from 10s of thousands of earthquakes are typically processed (Gritto et al., 2013a). tomoFDD uses absolute travel times to estimate the absolute location of earthquake hypocenters and to estimate the large-scale P- and S-wave velocity structure in the subsurface. Additionally, the code uses differential travel times, recorded at a common station for neighboring events, to estimate the relative hypocenter locations between neighboring events and to estimate the small-scale P- and S-wave velocity structure in the vicinity of these events. In the following, results of the seismic imaging will be presented to demonstrate the heterogeneity of the seismic P- and S-wave velocities as well as the Vp/Vs-ratio in the reservoir.

The depth distribution of the relocated earthquakes resulting from the 3D seismic inversion are presented in Figure 4. A few events at negative depth ranges between -1 and 0 km depth are visible. During the inversion, depth is measured with respect to mean sea level and because the topography at The Geysers is quite severe with elevations in excess of 1 km, the shallow location of these events is likely correct. The bimodal character of the depth distribution is well developed with events distributed in the shallower and deeper parts of the reservoir. This bimodal character has been reported in previous studies at The Geysers (e.g., Hartline et al., 2016, 2019; Lin and Wu, 2018).

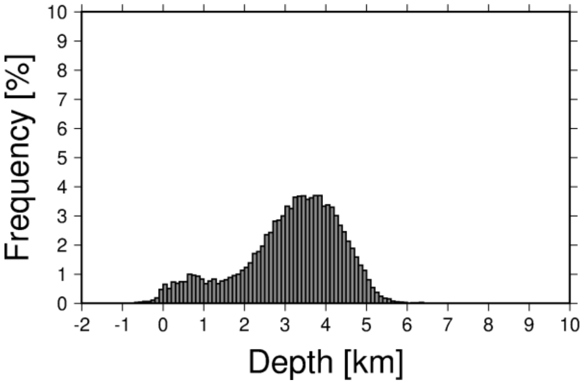

Figure 4: Histogram of hypocentral depth of 32,000 events recorded between May 2018 and June 2019 after 3D tomographic inversion.

The spatial distribution of the relocated earthquake hypocenters is presented in Figure 5. The figure shows the topography of The Geysers indicated by the gray shading and the hypocenters of the earthquakes color-coded as a function of depth. It can be seen that the events range from 0 km to 6 km depth and are located throughout the steam reservoir, which is indicated by the red polygon. While there exists a mix of shallow and deep events in the reservoir, the seismicity reveals a general trend of shallower events in the southeast and deeper events in the northwest. This trend is an indication of the extent of the geothermal reservoir to greater depth towards the northwest.

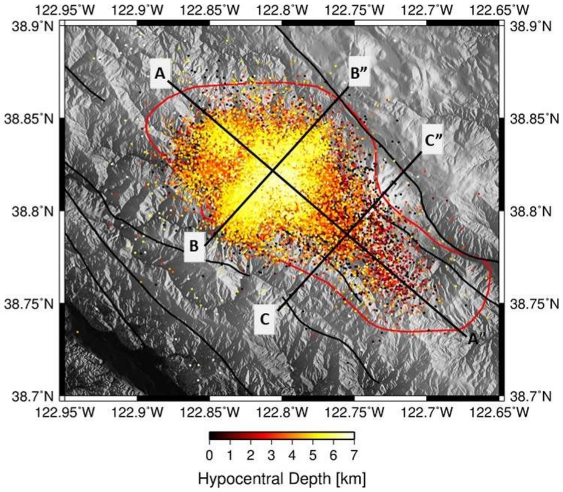

Figure 5: Map view of relocated seismicity resulting from 3D tomographic inversion. The seismicity represent more than 32,000 events recorded between May 2018 and June 2019. The profiles denote the locations of the cross sections in Figure 11.

The starting velocity model for the tomographic inversion was taken from the three-dimensional Vp and Vs model developed by Gritto et al. (2013a) for the entire Geysers area. This model serves as a general representation of the velocity heterogeneity in the reservoir, and it is expected that the tomographic imaging in the current project will improve the resolution of the older model due to the higher number of seismic stations currently available. The 3D seismic inversion is conducted by minimizing the misfit between theoretically calculated and observed travel times in a least squares sense. The theoretical travel times are computed based on the starting velocity model during the first iteration and on the updated models after each iteration. The misfit between calculated and observed travel times for the inversion as a function of the number of iterations is presented in Figure 6. The separate curves depict the misfit of the absolute and the weighted variance of the travel times. It can be seen that the curves decrease quickly with increasing number of iterations indicating that the misfit is minimized until it does not change further. In the current case, the misfit very little after the third iteration. This quick decrease is an indication that the starting model is already a good representation of the velocity distribution in the reservoir.

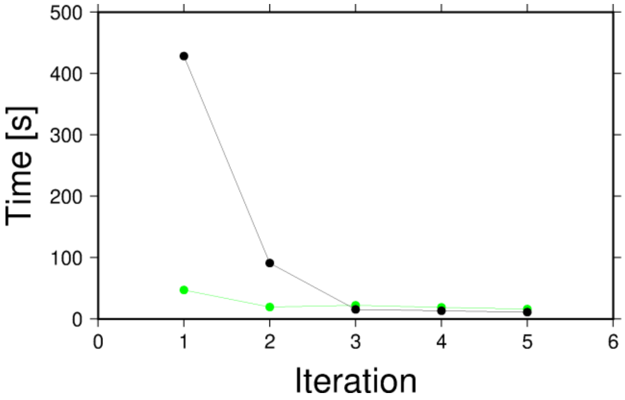

Figure 6: Misfit between synthetic and observed travel times for the inversion as a function of number of iterations. The black and green curves represent, respectively, the misfit of the absolute variance and the misfit of the weighted variance.

The Geysers geothermal reservoir is quite heterogeneous, and a view of the current reservoir model helps to identify the main geological features. Figure 7 reveals the 3D model developed by Hartline et al. (2016, 2019). It was developed to support the drilling program of Calpine, the operator of the reservoir. The model is based on logs from hundreds of boreholes and seismic earthquake data to delineate geological interfaces, the geothermal boundaries of the steam reservoir, and major fracture zones and flow paths. The main features visible in the model include the steam surfaces, which are represented by the colored contour lines, the top of the Hornfelsic Graywacke (translucent tan-colored interface), and the top of the Felsite (colored interface). The felsite is a granitic intrusion that is hypothesized to host the heat source of the reservoir. The steam contour lines indicate that the reservoir is shallowest in the southeast and dipping towards the northwest. This observation is supported by the trend of the geological interfaces, which are also dipping to the northwest. It is noted that the top of the Felsite reveals several peaks that protrude into the shallower parts of the reservoir, as will be revisited below.

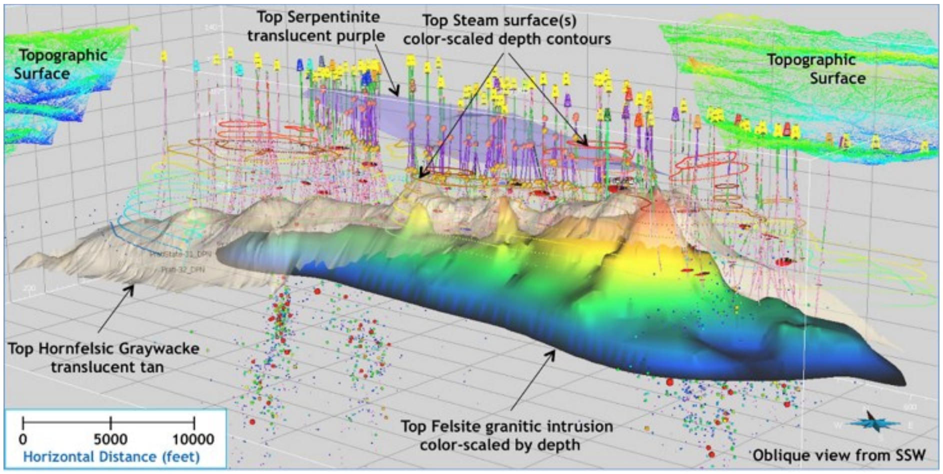

Figure 7: Three-dimensional structural model of The Geysers geothermal reservoir (from Hartline et al., 2016).

The inversion estimates for the P-wave velocity structure in the reservoir are presented for a selection of horizontal depth slices in Figure 8. Velocity estimates are only plotted for nodes that have sufficient resolution as defined by the derivative weight sum (DWS), which measures the total length of the ray paths through a given node in the reservoir. The estimates are only plotted for nodes that have a DWS value of at least 0.1 of the maximum DWS, such as in regions with high seismicity as shown in Figure 5. For this reason, resolution is highest in the central part and at central depths of the reservoir, decreases slightly towards the surface stations and tapers off in the deepest parts the reservoir and towards the boundaries of the steam field. In the shallow parts of the reservoir, between depths of 0.3 and 1.5 km, the P-wave velocity structure reveals intermediate values between Vp = 3.5 - 5.5 km/s, with lower values in the northwest and higher values in the southeast. They represent Hornfels and Graywacke units that are the main rocks the upper part of the reservoir (yellow and green colors). Along the southeastern boundary of the steam field velocities between Vp = 5.5 – 6.0 km/s become visible. They represent the top of the Felsite protruding into the reservoir above (blue-colored structure). The high velocity values expand spatially with increasing depth (2.1 – 3.3 km), as the Felsite takes up a larger volume in the reservoir (compare to Figure 7). The P-wave velocity increase with depth until maximum velocity values up to Vp = 6.0 km/s are observed in the central part of the reservoir. The spatial distribution of the high velocity anomaly represents the Felsite dipping from shallower depth in the southeast to greater depth in the center and the northwest of the reservoir.

The results of the S-wave velocity inversion are summarized in Figure 9. As before, velocity estimates are only plotted for nodes that have sufficient resolution as defined by the DWS. The number of S-wave phase arrival times in the data set is approximately 84% of the number of P-wave arrivals times. Therefore, the resolution of the S-wave velocity estimates is similar to that of the P-wave velocity estimates above. The spatial distribution of the S-wave velocity resembles that of the P-wave at shallow depth, with lower values in the northwestern part of the reservoir and higher velocities in the southeast. The Felsite is represented by S-wave velocities between 3.5 – 4.0 km/s, which show a dip from the southeast to the northwest of the reservoir. Overall, the S-wave velocities reveal a smoother spatial distribution that the P-wave velocities.

The ratio of Vp/Vs, or the Vp/Vs-ratio, has been used to interpret physical parameters in the subsurface. High Vp/Vs is often associated with fluid-filled fractured rock (Moos and Zoback, 1983, Gritto et al., 2004), while low Vp/Vs is related to dry, and gas filled rocks. In the case of The Geysers, high Vp/Vs relates to water saturated zones due to fluid injection and low Vp/Vs relates to regions where steam is predominantly present due to flashing of water to steam (Gritto et al., 2013b, Gritto and Jarpe, 2014). Thus, investigating Vp/Vs anomalies may yield conclusions about the state of the reservoir. The estimates for the Vp/Vs-ratio are shown in Figure 10. Because Vp/Vs-ratio is computed by taking the ratio of the P-wave and S-wave velocity estimates, the resolution for Vp/Vs-ratio is taken from the S-wave resolution as it is slightly lower than the P-wave resolution. Overall, the spatial heterogeneity of Vp/Vs is higher than that of Vp and Vs, because Vp/Vs is related to the fluid distribution in the reservoir, while the velocities are mostly related to geological units. In the shallowest parts of the reservoir low Vp/Vs-ratio (~1.4) can be found trending from the southeast to the northwest. These anomalies are likely indications of the presence of steam in the shallow subsurface as manifested by mineral deposits found at the surface along the Sulfur Creek Fault at the southwestern border of the reservoir and by steam vents in the Fumarole area adjacent to the Sulfur Creek Fault. With increasing depth, the low Vp/Vs-ratio becomes spatially more concentrated and slowly dips to the northwest. This trend is consistent with the trend of the steam reservoir, which is known to dip towards the northwest based on borehole data and from the distribution of the seismicity shown in Figure 5. A more detailed image of the steam reservoir is presented in Figure 11 below.

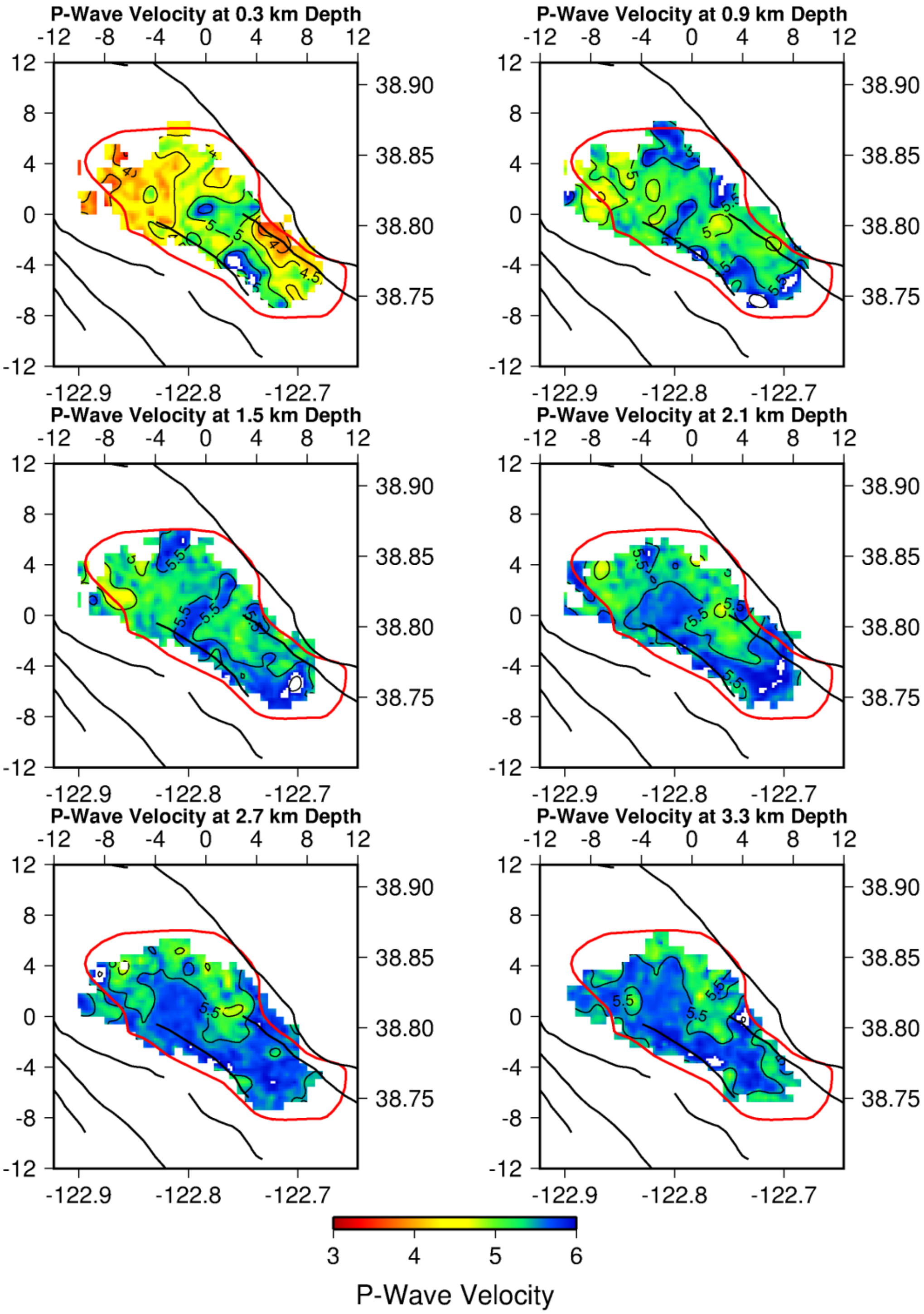

Figure 8: Horizontal slices of the P-wave velocity estimates from travel time inversion of more than 32,000 events. The estimates are only shown for regions that have sufficient ray coverage as determined by the derivative weight sum (DWS).

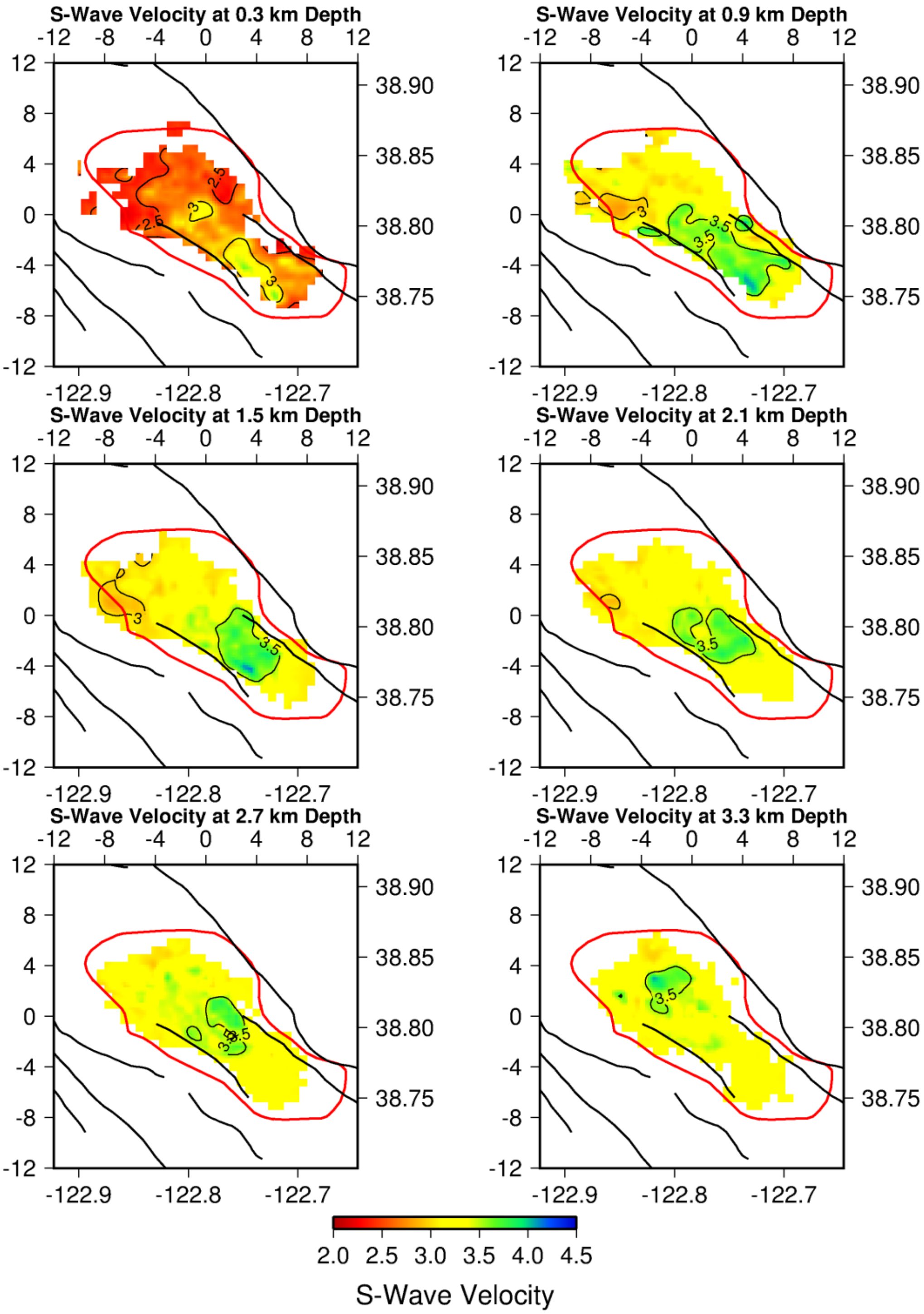

Figure 9: Horizontal slices of the S-wave velocity estimates from travel time inversion of more than 32,000 events. The estimates are only shown for regions that have sufficient ray coverage as determined by the derivative weight sum (DWS).

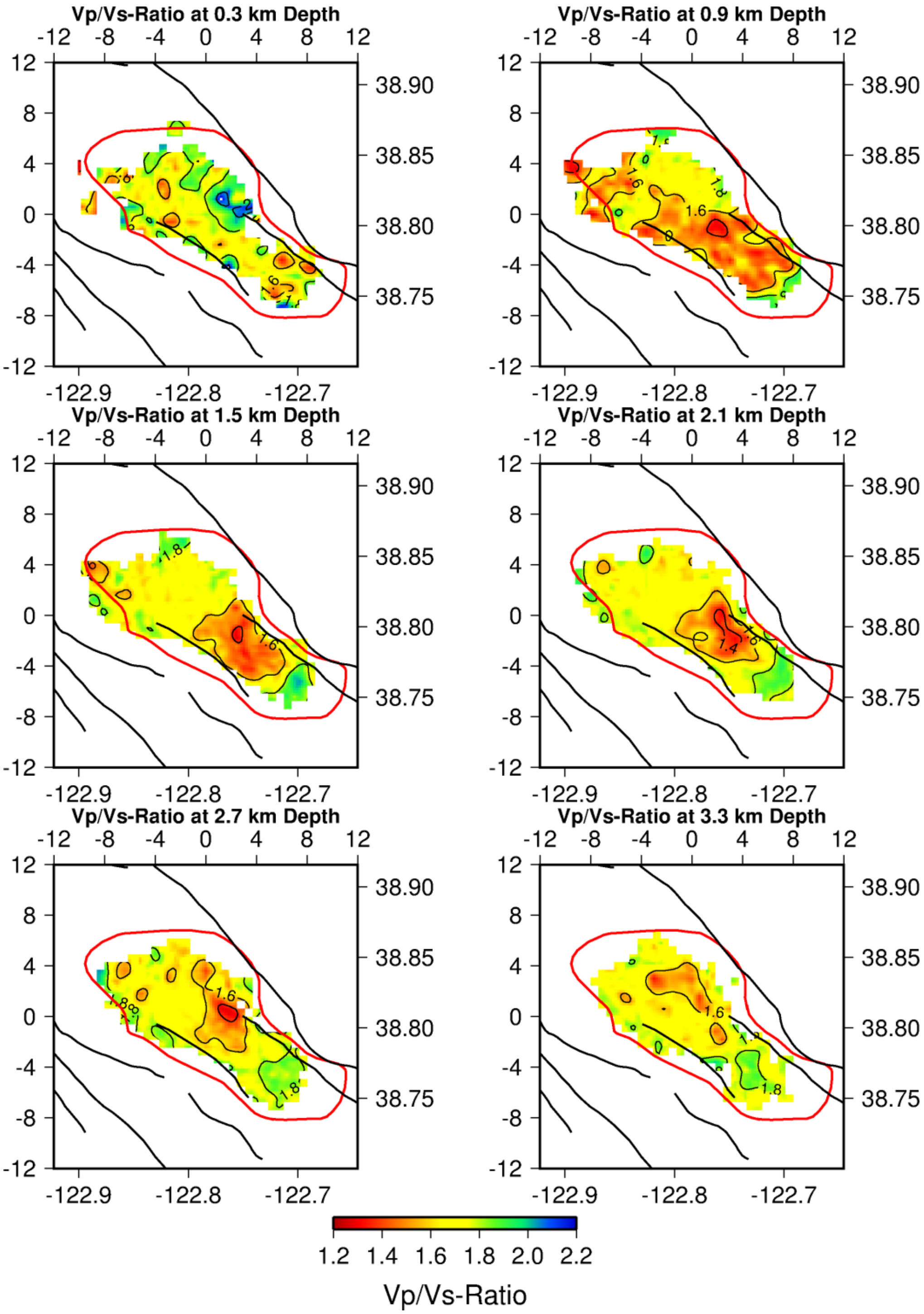

Figure 10: Horizontal slices of the Vp/Vs-ratio estimates from travel time inversion of more than 32,000 events. The estimates are only shown for regions that have sufficient ray coverage as determined by the derivative weight sum (DWS).

The cross sections in Figure 11 are located along the trend lines shown in Figure 5. Note that the color scale has been adjusted relative to Figure 10. Cross section A-A” displays the Vp/Vs-ratio in northwest-southeast direction and indicates the location of the steam reservoir by the red and orange colors (Vp/Vs = 1.4 – 1.6). It can be seen that the reservoir dips and thickens from the southeast (A”) towards the center, where it appears to split into a shallow and deep part towards northwest. The deepest part of the reservoir between 8 – 10 km distance correlates well with the deep seismicity in Figure 5. The Aidlin field, the northwestern most extension of The Geysers, is mapped by the shallow low Vp/Vs anomaly between 4 – 6 km distance. The Aidlin steam field appears to be dipping towards the southeast connecting with the upper and deeper sections of the reservoir between 6 – 8 km distance. Profiles B-B’ and C-C” show cross section in southwest-northeast direction. The low Vp/Vs anomaly in profile B-B” reveals the upper and lower steam reservoir in this region of The Geysers. Cross section C-C”, traversing the southeast Geysers, shows a low Vp/Vs anomaly that suggest a more shallow and compact steam field. The dashed lines in each cross section denote the upper and lower bounds of the steam field as observed by steam entries in boreholes. The relatively good match indicates the consistency between the borehole observations and the Vp/Vs images of this seismic tomography study.

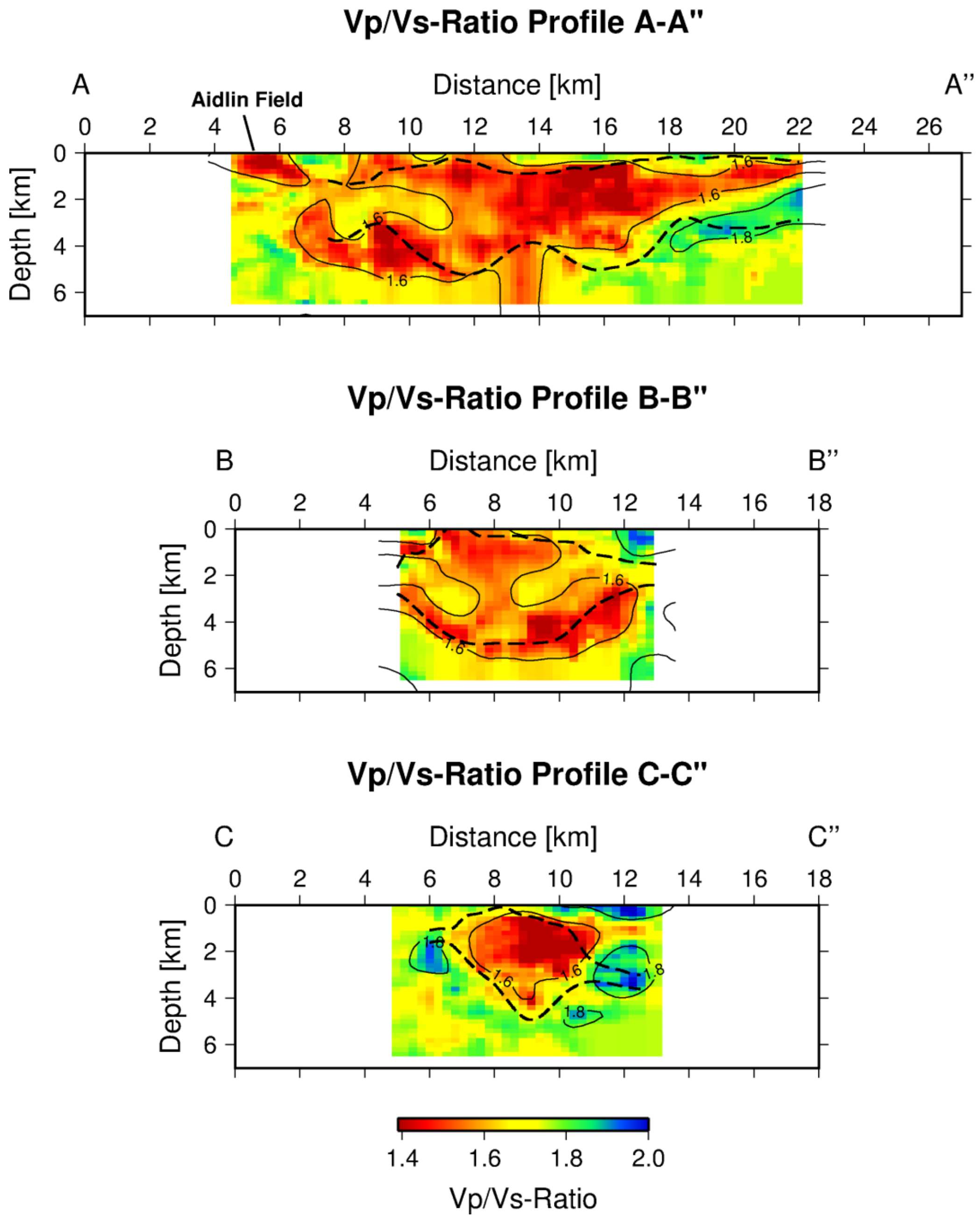

Figure 11: Vertical cross sections of the Vp/Vs-ratio estimates along the profiles shown in Figure 5.

4. CONCLUSIONS

Seismic studies of The Geysers geothermal reservoir have shown the extent of the steam field and the distribution of the seismicity in the past (Zucca et al., 1993; Julian et al., 1996; Gunasekera et al., 2003; Gritto et al., 2013a; Lin and Wu, 2018). These studies were based on seismic data recorded by the permanently installed seismic BG-network. The recent installation of a temporary cost-effective seismic network with high station density in the northwest Geysers has generated results that revealed the locations of steam and water pathways to support the development of a drilling program and to optimize the use of the resource in general (Gritto et al., 2020). In the current study and for the first time, both seismic networks were combined to generate a dataset that allows the highest resolution on a reservoir-wide scale to date. Specifically, the results indicate a compact steam field in the southeast Geysers that is slowly dipping toward the northwest while splitting into an upper and lower reservoir. The Aidlin steam field is clearly defined and its pathways to the upper and lower reservoir delineated. As a next step, the seismic data will be combined with MT data (Peacock et al., 2022) in a multi-physics data inversion to obtain reservoir structure with improved certainty in the structural controls and in the locations of water and steam in the reservoir. The joint inversion will be performed using workflows and algorithms that enforce structural similarity constraints between the different physical properties (Um et al., 2014).

REFERENCES

Dahm, T. and T. Fischer: Velocity ratio variations in the source region of earthquake swarms in NW Bohemia obtained from arrival time double-differences, *Geophys J. Int.*, Volume 196, Issue 2, February, 2014, Pages 957–970, doi: 10.1093/gji/ggt410., (2013).

Gritto, R.; T.M. Daley, and L.R. Myer: Joint Cross Well and Single Well Seismic Studies of CO2 Injection in an Oil Reservoir, *Geophysical Prospecting*, Vol. 52, pp. 323-339, (2004).

Gritto, R., S.H. Yoo and S.P. Jarpe: Three-dimensional seismic tomography at The Geysers geothermal field, CA, USA, *Proceedings,* 38th Workshop Geothermal Reservoir Engineering, SGP-TR-198, (2013a).

Gritto, R., S.H. Yoo and S.P. Jarpe: Seismic Imaging of reservoir structure at The Geysers geothermal reservoir, *Proceedings,* AGU 2013 Fall Meeting, S33D-2460, San Francisco, USA, 9–13 December 2013, (2013b).

Gritto, R. and S.P. Jarpe: Temporal variations of Vp/Vs-ratio at The Geysers geothermal field, USA, *Geothermics*, http://dx.doi.org/10.1016/j.geothermics.2014.01.012, (2014).

Gritto R., S.P. Jarpe, L.J. Hutchings, C. Ulrich, C.E. Layland-Bachmann, M. Schoenball, Y. Guglielmi, C.S. Hartline, K.T. Nihei, S. Nakagawa: Seismic Imaging of Spatial Heterogeneity at The Geysers Geothermal Reservoir Using a Cost-Effective Dense Seismic Network, *Proceedings,* 45th Workshop on Geothermal Reservoir Engineering, Stanford University, Stanford, CA, (2020).

Gunasekera, R.C., G.R. Foulger, and B.R. Julian: Reservoir depletion at The Geysers geothermal area, California, shown by four-dimensional seismic tomography, *J. Geophys. Res.*, **108**, 2134, doi:2110.1029/2001JB000638, (2003).

Julian B.R., A. Ross, G.R. Foulger, and J.R. Evans: Three-dimensional seismic image of a geothermal reservoir: The Geysers, California, *Geophys. Res. Lett.*, **23**(6), doi:10.1029/96GL03321, (1996).

Hartline, C.S., M.A. Walters, M.C. Wright, C.K. Forson, and A.J. Sadowski: Three-Dimensional Structural Model Building, Induced Seismicity Analysis, Drilling Analysis and Reservoir Management at The Geysers Geothermal Field, Northern California, *Proceedings*, 41st Workshop on Geothermal Reservoir Engineering, Stanford University, Stanford, California, February 22-24, SGP-TR-209, (2016).

Hartline, C.S., M.A. Walters, M.C. Wright: Three-Dimensional Structural Model Building Constrained By Induced Seismicity Alignments at The Geysers Geothermal Field, Northern California, *GRC Transactions*, **43**, pp. 24, (2019).

Hutchings, L., S. Jarpe, K. Boyle, H. Philson, and E. Majer: Inexpensive, Automated Micro-Earthquake Data Collection and Processing System for Rapid, High-Resolution Reservoir Analysis, Proceedings, Geothermal Resources Council, August, 2011, pp. 16, (2011).

Layland-Bachmann, C.E., R. Gritto, C.S. Hartline, L.J. Hutchings., S.R. Jarpe, K.T. Nihei and M. Schoenball: In-depth Analysis from Deployments of Low-Cost Seismic Instruments in the Geysers Geothermal Field, *Proceedings,* AGU 2019 Fall Meeting, San Francisco, CA, Dec. 9-13, S11F-0394, (2019).

Lin, G., and B. Wu: Seismic velocity structure and characteristics of induced seismicity at the Geysers Geothermal Field, eastern California, *Geothermics*, **71**, 225–233, (2018).

Moos D. and M. Zoback: In Situ Studies of Velocity in Fractured Crystalline Rocks, *J. Geophys. Res.*, **88**, B3, doi:10.1029/JB088iB03p02345, (1983).

Peacock, J.R., D. Alumbaugh, M. Mitchell, and C. Hartline: Repeat Magnetotelluric Measurements to Monitor the Geysers Steam Field in Northern California, *Proceedings*, 47th Workshop on Geothermal Reservoir Engineering, Stanford University, Stanford, CA, (2022).

Um, E., M. Commer and G. Newman: A strategy for coupled 3D imaging of large-scale seismic and electromagnetic data sets: Application to subsalt imaging, *Geophys.*, **79**, (2014).

Zhu, W., and G.C. Berosa, (2019), PhaseNet: a deep-neural-network-based seismic arrival-time picking method, *Geophys. J. Int.*, **216**, 261–273, (2019).

Zucca, J.J., L.J. Hutchings and P.W. Kasameyer: Seismic velocity and attenuation structure of The Geysers geothermal field, *Geotherm.*, **23**, 111-126, (1993)